PHYSICAL REVIEW E **71**, 030501(R) (2005)

Convection-driven pattern formation in phase-separating binary fluids

C. M. Pooley, Olga Kuksenok, and Anna C. Balazs
Department of Chemical Engineering, University of Pittsburgh, Pittsburgh, Pennsylvania 15261, USA
(Received 24 August 2004; revised manuscript received 20 January 2005; published 24 March 2005)

Using a thermal-lattice Boltzmann model, we examine the rich phase behavior that develops when partially miscible fluids evolve in the presence of a vertical temperature gradient, which encompasses the critical temperature T_c of the mixture. In particular, a binary *AB* fluid is confined between two plates in a gravitational field. The upper plate is fixed below T_c and hence, the nearby fluid phase separates into *A*-rich and *B*-rich domains. The lower plate is fixed above the temperature T_c, and the surrounding fluid is in the homogeneous phase. A coupling between convection (driven by the temperature gradient) and phase separation gives rise to unique pattern formation. A number of regimes are identified: regularly spaced stripes, convective steady-state columns, the periodic disturbance of these columns, and finally, chaotic dripping from the upper surface. These results highlight dynamical behavior in partially miscible mixtures.

DOI: 10.1103/PhysRevE.71.030501 PACS number(s): 64.75.+g, 47.54.+r, 47.20.Bp

The lava lamps of the early 1960s not only riveted our attention but also embodied fascinating physics, which actually plays a crucial role in the growth of semiconductor crystals, the processing of polymeric materials, and the formation of heterogeneous geological structures [1]. Common to all these systems is the evolution of complex fluids in the presence of a temperature gradient. We focus on one example of these intriguing systems: a phase-separating *AB* binary fluid that is confined between two plates, as depicted in Fig. 1(a). The bottom plate is hot and is above the fluid's critical temperature, T_c, while the top plate is cold and lies below T_c. In this scenario, the interplay between convection and phase separation can potentially lead to complex dynamical behavior. In particular, near the bottom plate, the mixture forms a single, homogeneous phase. Since this region is relatively hot, the fluid becomes less dense, and buoyancy drives it towards the top, colder plate, where the mixture phase separates into distinct domains. Gravity will act on this relatively heavier mixture and force the fluid downward, whereupon the entire process repeats. Therefore, one can expect not only the creation of convective patterns (similar to Rayleigh-Bénard convection), but also unique morphological patterns within the phase-separated fluid. In this paper, we use a lattice Boltzmann scheme to examine the structural evolution and dynamics of this system. Significant progress has been made in understanding convection in miscible binary fluids, as well as the role of interfacial phenomena in convection of immiscible fluids [2–4]. However, the system we study, which encompasses phase separation and thermal convection, has not been extensively examined. The few existing experimental studies have yielded specific cases of pattern formation [1,5]; however, these studies involved thin films, for which Marangoni convection is dominant and gravitational effects can be neglected. With respect to theoretical studies, Araki and Tanaka [6] examined the phase separation of a binary mixture subjected to a horizontal temperature gradient. Their model assumed that the density of the fluids does not depend on temperature. A unique feature of the model presented here is that we make no *ad hoc* assumptions about the functional dependencies of the density and temperature. Rather, we explicitly simulate all of the continuum equations that capture the behavior of the system. Our studies uncover regimes of spontaneous pattern formation, which are shown in Figs. 1(b)–1(f). More generally, the technique can potentially provide a powerful means of probing the interchange between temperature and structural evolution that occurs during the processing of a vast variety of materials.

To obtain the observed patterns, we simulate a two-dimensional system, with the y direction pointing upwards against gravity. The upper and lower edges of the system are fixed at temperatures $T_c-\Delta T/2$ and $T_c+\Delta T/2$, respectively. The *A* and *B* fluids have the same particle mass m and experience a repulsive interaction, whose strength is characterized by the parameter λ. The Landau free-energy functional for the system is

$$\Psi = \int \left(\psi + \frac{\kappa_\phi}{2}(\nabla \phi)^2 + \frac{\kappa_\rho}{2}(\nabla \rho)^2 - g\rho y \right) d\mathbf{r}. \tag{1}$$

The first term is the bulk free-energy density [7,8]

$$\psi = \frac{k_B T}{m}\left[\frac{\rho+\phi}{2}\ln\left(\frac{\rho+\phi}{2}\right) + \frac{\rho-\phi}{2}\ln\left(\frac{\rho-\phi}{2}\right)\right] + \lambda(\rho^2-\phi^2), \tag{2}$$

where T is temperature, $\rho=\rho_A+\rho_B$ is the total mass density, and $\phi=\rho_A-\rho_B$ is the mass density difference. The gradient terms, involving κ_ϕ and κ_ρ, represent the energy associated with surface tension, and the final term is the gravitational potential.

The dynamics of the system is determined by [9]

$$\begin{aligned} \partial_t \rho + \partial_\alpha(\rho u_\alpha) &= 0, \\ \partial_t(\rho u_\alpha) + \partial_\beta(\rho u_\alpha u_\beta) &= -\partial_\beta P_{\alpha\beta} + \partial_\beta \sigma_{\alpha\beta} - g\rho \hat{e}_{y\alpha}, \\ \partial_t(\rho \epsilon) + \partial_\alpha(\rho \epsilon u_\alpha) &= -\partial_\alpha q_\alpha + (-p_0\delta_{\alpha\beta} + \sigma_{\alpha\beta})\partial_\alpha u_\beta, \\ \partial_t \phi + \partial_\alpha(\phi u_\alpha) &= -\partial_\alpha i_\alpha. \end{aligned} \tag{3}$$

These equations ensure conservation of the total mass of each component, and the total momentum and energy. Here, u_α is the fluid velocity, $\sigma_{\alpha\beta}=\rho\nu(\partial_\alpha u_\beta+\partial_\beta u_\alpha)$ is the viscous stress tensor, g is the acceleration due to gravity, and $\hat{\mathbf{e}}_y$ is a unit vector in the y direction. The pressure tensor, in Eq. (3), is given by [7]

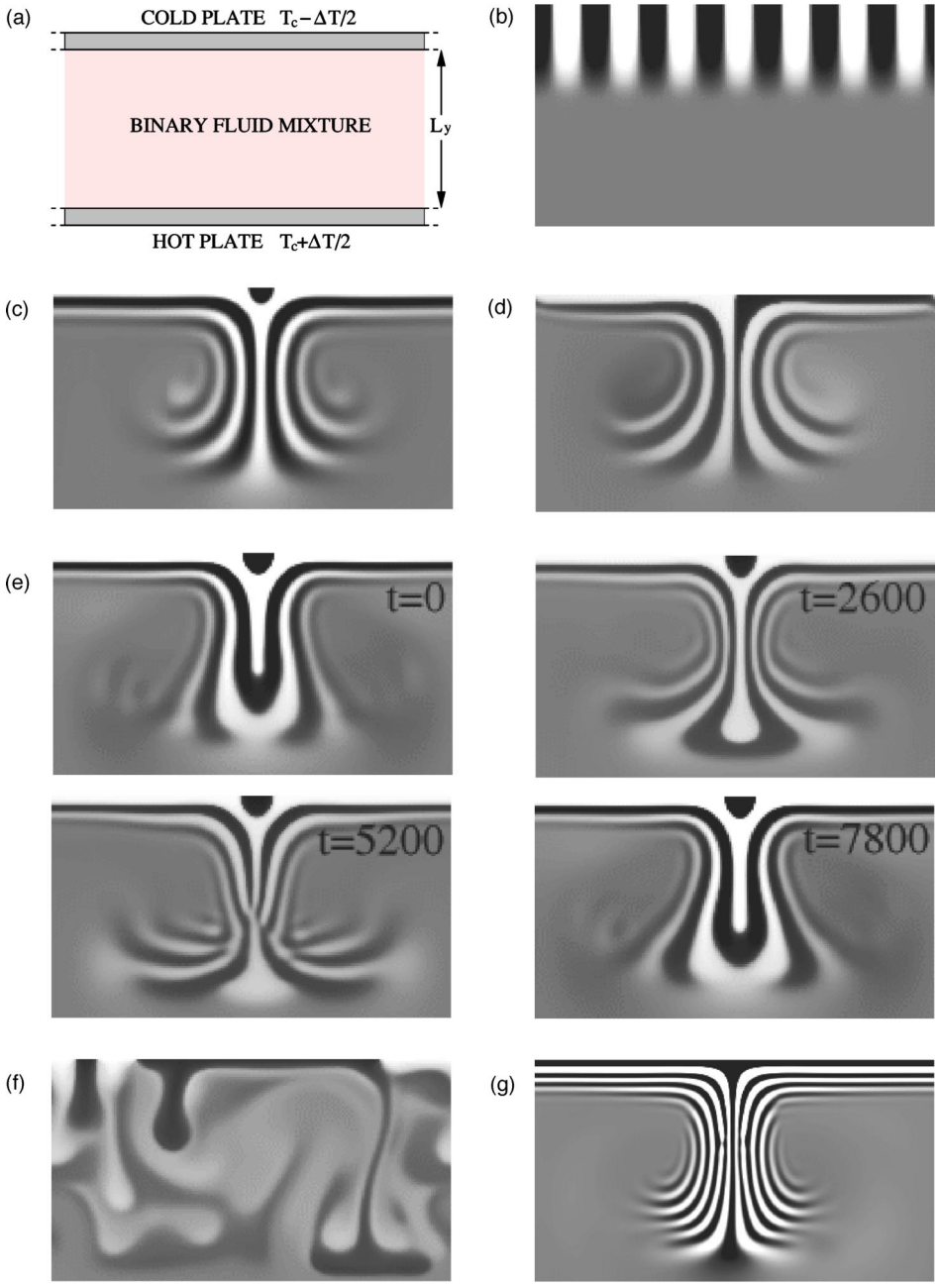

FIG. 1. (a) The system consists of a confined binary fluid, under the influence of gravity, heated from below and cooled from above. Periodic boundary conditions were used in the x direction, and the system size was chosen to allow one convective cell. (b)–(g) show the distribution of the density difference ϕ, where the white regions are A rich, the dark regions B rich, and the gray regions correspond to $\phi \sim 0$. A number of different regimes are ordered by increasing Rayleigh number [see Eq. (11)]: (b) regular stripes with no Rayleigh-Bénard convection (Ra=1719), (c) symmetric steady-state columns (Ra=6875), (d) asymmetric steady-state columns (Ra=6875), (e) periodic disturbance of the columns (the four frames show the evolution through one period, with time t measured in simulations time-steps, Ra=14 732), and (f) chaotic dripping from the upper surface ($\mathrm{Ra}=5.1\times10^5$). (g) A system that is double the size of (c) ($L_x=360$, $L_y=200$), with the same Rayleigh number.

$$P_{\alpha\beta} = p\,\delta_{\alpha\beta} + \kappa_\phi \partial_\alpha \phi \partial_\beta \phi + \kappa_\rho \partial_\alpha \rho \partial_\beta \rho, \tag{4}$$

where

$$p = p_0 - \kappa_\phi \phi \nabla^2 \phi - \frac{\kappa_\phi}{2} |\nabla \phi|^2 - \kappa_\rho \rho \nabla^2 \rho - \frac{\kappa_\rho}{2} |\nabla \rho|^2, \tag{5}$$

and the bulk pressure and chemical potential are

$$p_0 = (k_B T/m)\rho + \lambda(\rho^2 - \phi^2), \tag{6}$$

$$\mu_\phi = \frac{k_B T}{2m} \ln\left(\frac{\rho+\phi}{\rho-\phi}\right) - 2\lambda\phi - \kappa_\phi \nabla^2 \phi. \tag{7}$$

The internal energy per unit mass, ϵ, is related to the temperature by

$$\rho\epsilon = c_v (k_B T/m)\rho + \lambda(\rho^2 - \phi^2), \tag{8}$$

where $c_v = \frac{3}{2}$ is the specific heat per particle at constant volume. The first term comes from equipartition of energy, and the second comes from the potential energy associated with the repulsive interaction λ. Hence, there is a latent heat associated with transformations between the phase-separated and homogeneous states.

In the most general terms, the density difference flux, i_α, and the thermal flux, q_α, can be written as [9]

$$i_\alpha = -\alpha \partial_\alpha \mu_\phi - \beta \partial_\alpha T, \tag{9}$$

$$q_\alpha = \tfrac{1}{2}(\mu_\phi + \beta T/\alpha) i_\alpha - k \partial_\alpha T. \tag{10}$$

We ignore concentration diffusion resulting explicitly from temperature gradients, hence, we set $\beta=0$. The first term on the right-hand side of Eq. (10) comes from energy transport

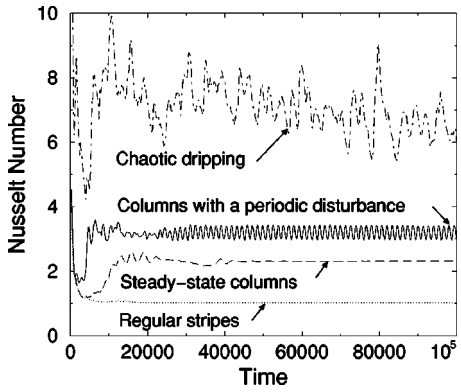

FIG. 2. The Nusselt number as a function of time.

from interparticle diffusion, and the last term from energy conduction, where k is the thermal conductivity. The mobility α is itself a function of the density difference. The simplest choice, which is used in these simulations, is $\alpha = \alpha_d(\rho^2 - \phi^2)$, where α_d is a constant. Note that in the limit when $\phi = \pm\rho$ (the pure phases), no diffusion occurs and hence, $\alpha = 0$.

A thermal-lattice Boltzmann algorithm [10] is used to simulate the continuum equations [see Eq. (3)]. The scheme is an extension of that proposed by Palmer and Rector [11] for a single component fluid with no gravitational force. Simulations were performed using a system of size $L_x = 180$ and $L_y = 100$ lattice units, with periodic boundary conditions in the x direction, and nonslip, fixed temperature, neutrally wetting boundaries on the upper and lower plates. In each simulation, the initial state was given by $\rho = \rho_0[1 + (\Delta T/2T_c)(y/L_y)]$ (to ensure that the initial pressure is approximately constant), $\phi = 0$, and $T = T_c - (\Delta T/L_y)y$, with a small random noise added to each. y is measured relative to the center between the plates. Unless otherwise stated, we use the parameters $\rho_0 = 1$, $g = 0.01$, $\alpha_d = 0.2$, $k_B = 1$, $k = 1$, $\kappa_\phi = 0.2$, $\kappa_\rho = 0.2$, $m = 1$, and $\lambda = 2$. By setting $\mu_\phi = 0$ in Eq. (7), we derive the critical temperature $T_c = 2m\rho_0\lambda/k_B = 4$. The lattice cell size was $\Delta x = 1$ and the time step was taken to be $\Delta t = 0.2$, which is sufficiently small to allow all the simulations to be numerically stable. Simulations were performed for 2×10^6 time steps, which was large enough to observe the long-time behavior of the system. The viscosity ν and temperature difference ΔT were varied between simulations.

At early times, fluid at a temperature below T_c phase separates via spinodal decomposition. In the long-time limit, a number of topologically distinct morphologies are identified. Examples of these are shown in Fig. 1. First, we describe the main features of each regime, and then we construct a phase diagram to clarify the phase boundaries between regimes.

When the viscosity of the fluid is sufficiently high, the phase-separated fluid forms regular stripes of alternating A- and B-rich regions. This is illustrated in Fig. 1(b), where $\nu = 3$ and $\Delta T = 0.5$. Interestingly, the width-to-height ratio of the domains was found to be independent of simulation parameters. Because of the temperature gradient, we observe the Marangoni effect forcing fluid down the interfaces, and consequently rising up the middle of each domain. Figure 2 shows the time evolution of the dimensionless Nusselt number, $\mathrm{Nu} = fL_y/k\Delta T$, which gives the energy flux between the two plates, f, relative to a purely conducting state. The curve saturates at $\mathrm{Nu} \simeq 1.02$, suggesting that the induced velocities are small; however, they are still important in forming the regular domain spacing. For instance, if we set the fluid velocity to zero, such that the system is governed only by the Cahn-Hilliard equation, then we do not see this regular patterning. Instead, domains coarsen in time to reduce the global interfacial energy. The regime in Fig. 1(b) suggests that an applied temperature gradient can be exploited to create patterned surfaces.

Figure 1(c) shows a final steady-state morphology when $\nu = 1.5$ and $\Delta T = 1$. Fluid near the upper surface orders into alternating A and B horizontal bands. The phase-separated fluid is heavier than that surrounding it, and is forced by gravity downward, through columns. The velocity flow field is similar to that observed in single-component Rayleigh-Bénard convection. The pattern in ϕ is advected with the fluid to produce the striped column structure. Figure 1(d) shows another possible steady-state situation. In this case, the order of A and B downward from the upper surface is different on either side of the column, and asymmetric columns are produced. This picture was taken from part of a larger simulation containing six columns and using the same parameters as above. In large systems, both symmetric and asymmetric columns are observed. In the case of neutral wetting, the local ordering of phases near the surface results from the initial randomness. If the upper surface is preferentially wetted by one component, then only symmetric columns form.

For lower viscosities, the columns become unstable, resulting in a regime we call "periodic disturbances;" a typical example of this is given in Fig. 1(e) (here $\nu = 0.7$ and $\Delta T = 1$). The four frames show the time evolution of the system through one period. It is probable that this instability results from a competition between gravity, pushing the denser fluid down, and surface tension, which drives a reduction in total interface length. The periodicity is seen more clearly if we examine the Nusselt number in Fig. 2. Periodic oscillations also occur in asymmetric columns. If the viscosity is reduced further, then the amplitude of the oscillation increases and the periodicity is lost.

Another possible scenario is shown in Fig. 1(f), for which $\nu = 0.4$, $\Delta T = 1$, and $k = 0.05$. When the thermal conductivity becomes too low, the system becomes unstable with respect to forming columns. Drips of phase-separated fluid are observed to come from the upper surface. The system exhibits chaotic behavior, which is reflected in the chaotic fluctuations in the Nusselt number.

Figure 1(g) shows the result of doubling the size of the system used in Fig. 1(c), and using the parameters $g = 0.0025$ and $\nu = 3$, such that the Rayleigh number and interface width are kept the same. An approximate doubling of stripe number is observed, suggesting that stripe width is proportional to interface width.

Figure 3 shows a phase diagram for the system, using as variables the temperature difference, ΔT, and the viscosity, ν. The symbols indicate points where simulations have been performed, and the shaded regions are shown to clarify the

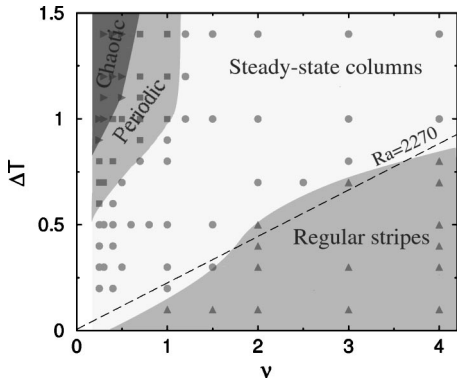

FIG. 3. The flow regimes for different viscosity, ν, and temperature difference, ΔT. The periodic and chaotic areas refer to periodic and chaotic disturbances of the columns, respectively. In the regular stripes region, Rayleigh-Bénard convection is not observed.

approximate areas for each of the different regimes. We point out a number of features within this diagram. First, within the periodic region, the oscillation period varied from approximately 5000 time-steps at $\nu=0.3$, to 10 000 time steps at $\nu=1$, and the size of the oscillations became increasingly large as the chaotic regime was approached. Second, because of numerical instability, it was not possible for the viscosity to be reduced below $\nu=0.25$. This means there is no region in this diagram referring to the very large Rayleigh number situation illustrated in Fig. 1(f) (for this to be observed, the thermal conductivity was dramatically reduced). Third, close to the line between the "regular stripes" and the "steady-state columns" regions, there were intermediate states, in which the boundary between the phase-separated and homogeneous regions in Fig. 1(d) exhibited wavelike oscillations.

Since the velocity profile is similar to that observed in Rayleigh-Bénard convection, it is natural to assume that the Rayleigh number, which we define as

$$\mathrm{Ra} = c_v g \Delta\rho L_y^3 / k\nu, \tag{11}$$

can be used to characterize the system. Here, $\Delta\rho$ is the density difference in equilibrium between the top and bottom of the system. Figure 3 shows the approximate critical Rayleigh number $\mathrm{Ra}^{crit}=2270$ for stability against Rayleigh-Bénard convection. This is somewhat larger than that analytically derived for a single component fluid, $\mathrm{Ra}^{crit}\simeq 1707$. In part, this results from the surface tension between the domains in Fig. 1(b), which inhibits convection, and is characterized by the Bond number $\mathrm{Bo}=g\Delta\rho L_y^2/\sigma$. However, in the simulations, the Bond number is high, $\mathrm{Bo}\sim 100$, suggesting that the effect of surface tension is not sufficient to explain the discrepancy. This will be the subject of future research [10]. We note that the Marangoni number, $\mathrm{Ma}=\rho c_v(d\sigma/dT)\Delta T L_y/k\nu$, where σ is the surface tension, was typically $\mathrm{Ma}\sim 10$. This is less than the critical value $\mathrm{Ma}^c\sim 80$, implying that there is no Marangoni convection.

Actual, physical parameters can be related to system parameters via the kinematic viscosity, $\nu_r=\nu(\Delta t/\Delta x^2)\times(\Delta x_r^2/\Delta t_r)$, the thermal diffusivity, $k_r^d=(k/c_v\rho_0)(\Delta t/\Delta x^2)\times(\Delta x_r^2/\Delta t_r)$, and the gravitational acceleration, $g_r=g(\Delta t^2/\Delta x)(\Delta x_r/\Delta t_r^2)$, where the subscript r denotes that the value is in S.I. units. A typical fluid has $\nu_r=10^{-6}\ \mathrm{m^2\ s^{-1}}$, and $k_r^d=10^{-7}\ \mathrm{m^2\ s^{-1}}$, and $g_r=9.8\ \mathrm{m\ s^{-2}}$. By approximately matching these parameters, we obtain the lattice size $\Delta x_r\simeq 10^{-5}$ m, corresponding to $L_{y_r}\simeq 1$ mm.

It is worth noting that in phase-field models, such as the lattice Boltzmann method, the interface width cannot be reduced below 3 or 4 lattice units (around 30 μm in the example above) without the introduction of unphysical, nonisotropic disturbances of the velocity. However, in real systems, the interface width can be of the order of nanometers to hundreds of nanometers (depending on the depth of the quench). Therefore, since Fig. 1(g) suggests that stripe width is proportional to interface width, in an experiment, we would expect to observe a very large number of alternating layers of A and B fluid [12].

To summarize, we find that by convecting a binary fluid through its critical transition temperature, we observe unique pattern formation. Since temperature gradients, surface tension and gravity play important roles during processing, the findings reveal phenomena that could be affecting the fabrication of a large class of materials. At the same time, the findings also reveal how these factors can be manipulated to create dynamically driven structures and thereby, create materials with unique morphologies, which can provide additional functionality to the final products.

[1] J. Kumaki, T. Hashimoto, and S. Granick, Phys. Rev. Lett. **77**, 1990 (1996), and references therein.

[2] M. C. Cross and P. C. Hohenberg, Rev. Mod. Phys. **65**, 851 (1993).

[3] A. Nepomnyashchy, M. G. Velarde, and P. Colinet, *Interfacial Phenomena and Convection* (Chapman and Hall/CRC, Boca Raton, FL, 2002).

[4] F. H. Busse and G. Schubert, J. Fluid Mech. **46**, 801 (1971).

[5] M. Assenheimer, B. Khaykovich, and V. Steinberg, Physica A **208**, 373 (1994).

[6] T. Araki and H. Tanaka, Europhys. Lett. **65**, 214 (2004).

[7] M. R. Swift, E. Orlandini, W. R. Osborn, and J. M. Yeomans, Phys. Rev. E **54**, 5041 (1996).

[8] The model does not account for hard sphere interactions between particles, yielding a fluid that is more compressible than a physical liquid. This degree of compressibility was necessary to ensure the stability of the simulation over sufficiently long time-steps; however, the results remain qualitatively the same for less compressible fluids.

[9] L. D. Landau and E. M. Lifshitz, *Fluid Mechanics*, 2nd ed. (Pergamon Press, New York, 1987).

[10] C. M. Pooley, O. Kuksenok, and Anna C. Balazs (unpublished).

[11] B. J. Palmer and D. R. Rector, Phys. Rev. E **61**, 5295 (2000).

[12] However, it is possible that there exists some stripe-coarsening process at a very high stripe number, which would reduce the large interfacial energy. In addition, Brownian noise, which was not included in these simulations, may be important for stripe stability.